Enhanced Retention and Cellular Uptake of Nanoparticles in Tumors by Controlling Their Aggregation Behavior

Xiangsheng Liu, Yangjun Chen, Huan Li, Nan Huang, Qiao Jin, Kefeng Ren, and Jian Ji*

MOE Key Laboratory of Macromolecular Synthesis and Functionalization, Department of Polymer Science and Engineering, Zhejiang University, Hangzhou 310027, China

ABSTRACT Effective accumulation of nanoparticles (NPs) in tumors is crucial for NP-assisted cancer diagnosis and treatment. With the hypothesis that aggregation of NPs stimulated by tumor microenvironment can be utilized to enhance retention and cellular uptake of NPs in tumors, we designed a smart NP system to evaluate the effect of aggregation on NPs' accumulation in tumor tissue. Gold nanoparticles (AuNPs, ~16 nm) were facilely prepared by surface modification with mixed-charge zwitterionic self-assembled monolayers, which can be stable at the pH of blood and normal tissues but aggregate instantly in response to the acidic extracellular pH of solid tumors. The zwitterionic AuNPs exhibited fast, ultrasensitive, and reversible response to the pH change from pH 7.4 to pH 6.5, which enabled the AuNPs to be well dispersed at pH 7.4 with excellent stealth ability to resist uptake by macrophages, while quickly aggregating at pH 6.5, leading to greatly enhanced uptake by cancer cells. An *in vivo* study demonstrated that the zwitterionic AuNPs had a considerable blood half-life with much higher tumor accumulation, retention, and cellular internalization than nonsensitive PEGylated AuNPs. A preliminary photothermal tumor ablation evaluation suggested the aggregation of AuNPs can be applied to cancer NIR photothermal therapy. These results suggest that controlled aggregation of NPs sensitive to tumor microenvironment can serve as a universal strategy to enhance the retention and cellular uptake of inorganic NPs in tumors, and modifying NPs with a mixed-charge zwitterionic surface can provide an easy way to obtain stealth properties and pH-sensitivity at the same time.

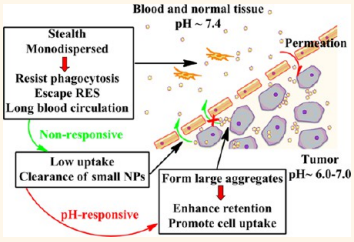

KEYWORDS: gold nanoparticles · mixed-charge zwitterionic · pH-responsive · aggregation · tumor accumulation

The application of nanoparticles (NPs) in biomedicine has provided new noninvasive strategies for the diagnosis and treatment of cancer.[1−9] Nanoparticles can be designed to realize various inspiring functions *in vivo*, but only if they are effectively accumulated at malignant tumor sites, which is not an easy task due to the complexity of biological systems.[3,9−11] The leaky tumor vasculature endothelium (100−1000 nm) provides the feasibility for NPs to permeate into solid tumors, and the lack of functional lymphatic drainage in tumor tissue makes it difficult to efficiently remove the permeated NPs, which are thus retained in tumors. This phenomenon, termed the enhanced permeability and retention (EPR) effect, has served as a primary rationale for the delivery of nanoparticles to solid tumors.[12,13] The accumulation of NPs in tumors mediated by the EPR effect strongly depends on the physicochemical characteristics of nanoparticles, especially size and surface properties.[13,14] For NPs without proper surface modification, once they enter the bloodstream, they are susceptible to nonspecific plasma protein adsorption, known as opsonization.[15−17] The opsonized nanoparticles can be easily captured by the reticuloendothelial system (RES) or mononuclear phagocytic system (MPS), leading to a rapid clearance of nanoparticles from the blood. Without a long blood circulation time, nanoparticles have no chance to achieve enough permeation to tumor tissue through the leaky tumor vasculature. Surface modification of nanoparticles with polyethylene glycol (PEG)[18−24] or zwitterionic groups[23,25−31] is demonstrated to be the most effective and preferred method for avoiding clearance of NPs by the RES. The modified NPs are considered to be "stealth" NPs with a long blood half-life. Besides surface property, size effect plays an importance role in the accumulation of the "stealth" NPs in tumors. It is reported that nanoparticles with a diameter between 30 and 200 nm can accumulate more effectively inside tumor tissues.[10] Perrault *et al.* have demonstrated that large

* Address correspondence to jijian@zju.edu.cn.

Received for review May 1, 2013 and accepted June 25, 2013.

Published online June 25, 2013
10.1021/nn402201w

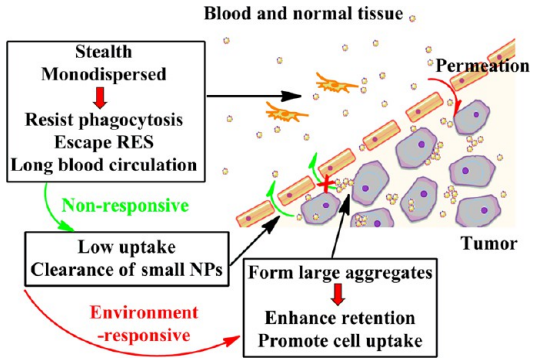

Scheme 1. Schematic illustration of the hypothesis that retention and cellular uptake of small nanoparticles in tumors can be enhanced by inducing aggregation of nanoparticles in the tumor environment.

nanoparticles (100 nm) modified with PEG do not extravasate far beyond the blood vessel because they remain trapped in the extracellular matrix between cells, while small nanoparticles (20 nm) have the ability to penetrate deep into the tumor tissue but are not retained beyond 24 h before being cleared into the surrounding tissues.[21] Besenbacher *et al.* also have shown that small nanoparticles could re-enter the bloodstream and deplete the amount retained within tumors.[22] This implies that particles with larger diameters may benefit from a lower migration rate through the interstitial space, allowing greater accumulation, but also face the problem of inefficient penetration into the tumor.

In fact, many nanoparticles, especially inorganic nanoparticles, that are currently being studied for biomedical applications have a relatively small size, less than 50 nm, such as quantum dots,[1] magnetic nanoparticles,[7] and gold nanoparticles.[8] Moreover, the stabilization of larger nanoparticles is a more difficult task than that of smaller nanoparticles.[32−34] Therefore, enhancing the retention of small particles in tumors will be of great importance for realizing their unique functions in cancer diagnosis and treatment. For this purpose, we hypothesize that retention and cellular uptake of small nanoparticles in tumors can be enhanced by stimulated aggregation of nanoparticles in tumor sites by certain factors of the tumor microenvironment (Scheme 1). During circulation in the blood, stable nanoparticles with stealth surfaces show prolonged circulation times and can leak into tumor sites through the EPR effect. Once nanoparticles extravasate into tumor tissue, owing to the tumor stimuli, the NPs will aggregate and hence be trapped in the tumor site due to the increased sizes of the aggregates, leading to enhanced retention of NPs in the tumor. The NP aggregates are expected to sedimentate at the tumor interstitium, which increases the uptake of NPs by cancer cells due to the direct interaction between the aggregates and cells.[35−37] The intracellular uptake of NPs will further enhance the retention effect, which can also be utilized for realizing the function of NPs within cells more than in tumor interstitium alone.

To achieve the aggregation of inorganic nanoparticles inside tumors, designing nanoparticles that can respond to certain tumor microenvironments will be a good choice. Stimulus-responsive nanoparticles for tumor targeting have attracted extensive attention so far.[38,39] One of the most promising stimuli is the pH of the tumor microenvironment. The extracellular pH (pHe) of most tumors is more acidic (pH 6.0−7.0) than that of extracellular fluid/blood in normal tissue (pH 7.2−7.4), resulting from hypoxia, anaerobic/aerobic glycolysis, and ion channel disregulation.[40−44] Polymer-assembled nanoparticles[45−49] or nanoparticles encapsulated in a polymer[50−52] with super pH sensitivity for targeting the extracellular or intracellular pH of tumors have been well developed. Despite these remarkable advances, it is still a considerable challenge to design an effective pH-smart targeting system for inorganic nanoparticles merely by surface modification. Inorganic nanoparticles with pH sensitivity between dispersion and aggregation could be easily prepared by surface modification with various ligands.[53−59] However, few of them are suitable for tumor targeting. First, they have a pH-responsive range not covering the tumor's pH extent where the nanoparticles should undergo an accurate and quick phase transition in a complex biological system with a relatively narrow range of pH difference (<1 unit between normal and disease tissue).[52,60] Second, they may not possess a "stealth" surface when circulating in blood and normal tissue, which is a prerequisite for pH-responsive nanoparticles to target an acidic tumor microenvironment *in vivo*.[49,51]

Even though PEGylation-based pH-sensitive inorganic nanoparticle systems have been successfully developed,[50,51] the special design of PEG is needed as the inherent PEG chain itself has no pH sensitivity. Distinctly, for a zwitterionic system comprising both positively and negatively charged groups, there are many ways to design pH-responsive systems with only one of or both the groups protonated or deprotonated, such as carboxyl and amino groups. We observed the pH sensitivity of nanoparticles modified with 11-mercaptoundecylphosphorylcholine in previous work,[34,61] finding out the pH-responsive range is between 4 and 6, which is not suitable for tumor pHe targeting. At present, few studies on the pH sensitivity of the most commonly used single-component zwitterionic groups, such as phosphorylcholine, sulfobetaine, and carboxybetaine, have been reported due to their fixed composition. Except for single-component zwitterionic species bearing both positive and negative charges in the same molecule, a surface fabricated with a combination of opposite charges in separate ligands in near equal amount can also exhibit excellent nonfouling properties.[62−64] Recently, the mixed-charged zwitterionic

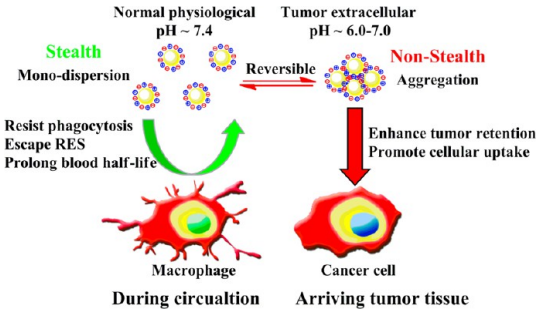

Scheme 2. Schematic illustration of the targeting of acidic tumor microenvironment by pH-responsive mixed-charge zwitterionic AuNPs (symbols on the NP (yellow color) surface mean positively charged groups (blue color) and negatively charged groups (red color) localized on the NP surface simultaneously). During circulation in the blood, the nanoparticles with small size and the zwitterionic surface exhibit a prolonged circulation time and hence can leak into tumor sites *via* the EPR effect. Arriving at the tumor site, stimulated by the tumor extracellular pH (pHe), the zwitterionic AuNPs form aggregates and sedimentate in the tumor space, leading to enhanced retention and cellular uptake of NPs in the tumor.

strategy was successfully utilized to stabilize gold nanoparticles[33,65] and tantalum oxide nanoparticles.[26] In preliminary work, we modified 16 nm gold nanoparticles with a combination of trimethylammonium groups and sulfonic groups, which were stable over the entire pH range because both kinds of ligands on NPs are strong electrolytes with permanent positive and negative charges.[17] It can be easily imagined that if we change the groups on the mixed-charge surface from strong electrolytes to weak electrolytes, we could obtain a pH-sensitive zwitterionic surface. Here, we prepared pH-sensitive mixed-charge zwitterionic AuNPs with modification of mixed self-assembled monolayers (SAMs) of weak electrolytic 11-mercaptoundecanoic acid and strong electrolytic (10-mercaptodecyl)trimethylammonium bromide. In this way, we can obtain mixed-charge zwitterionic AuNPs with desired pH sensitivity especially for the targeting of acidic tumor microenvironments. The AuNPs can disperse well in the pH range of blood and normal tissues, acting as "stealth" NPs when circulating in the body due to the nonfouling zwitterionic property. The NPs can also aggregate instantly in the acidic pH range of tumors (Scheme 2). The formation of large aggregates is expected to enhance the retention of NPs in tumor tissue both by being trapped in the extracellular matrix and by being internalized by tumor cells owing to the enhanced interaction between cells and NPs, since the NP surface is no longer "stealth" after sedimentation on cells.

RESULTS AND DISCUSSION

To prepare pH-sensitive zwitterionic AuNPs, mixtures of weakly electrolytic negative 11-mercaptoundecanoic acid (HS-C10-C) and strongly electrolytic positive (10-mercaptodecyl)trimethylammonium bromide

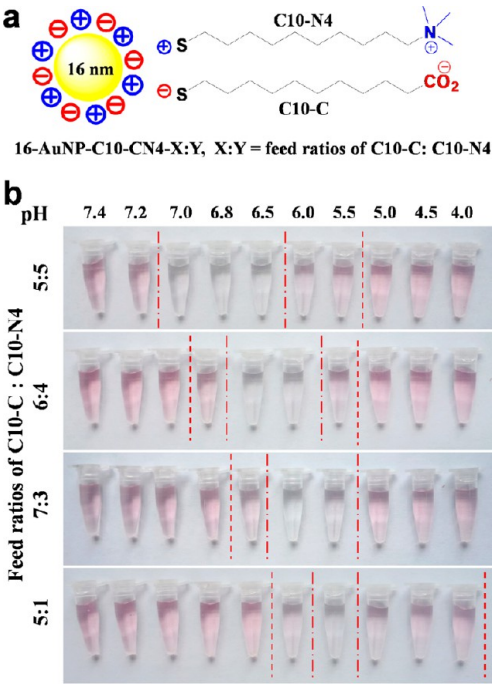

Figure 1. (a) Schematics of pH-responsive zwitterionic gold nanoparticles modified with mixed-charge thiols (16-AuNP-C10-CN4-X:Y, not to scale). (b) Digital images of 16-AuNP-C10-CN4-X:Y at different pH conditions. Clear red color means excellent dispersion of gold nanoparticles. The red lines are drawn to make the images show more clearly. Samples between two dash dot lines are aggregated NPs. Samples between a dash dot line and a dash line are partially aggregated ones. The others are nonaggregated NPs.

(HS-C10-N4) with different ratios were used to modify 16 nm citrate-capped AuNPs (Figure 1a; in the following discussion, these AuNPs are referred to as 16-AuNP-C10-CN4-X:Y, C10-C means a carboxylic group at the end of a 10-carbon (C10) alkyl chain, N4 means a quaternary ammonium group (the number 4 means quaternary); C10-CN4 means the ligands immobilized on NPs are a mixture of C10-C and C10-N4; X:Y means molar feed ratios of HS-C10-C to HS-C10-N4). When the feed ratio of carboxylic ligand to quaternary ammonium ligand ranges from 5:5 to 5:1, the modified AuNPs showed different aggregation transition pH values ranging from 7.0 to 5.5 (Figure 1b). Taking 16-AuNP-C10-CN4-5:5 as an example (Figure S1), transmission electron microscopy (TEM) images of the AuNPs at different pH values showed that AuNP aggregates have sizes ranging from ~50−100 nm (loosely aggregated, such as at pH 5.5) to ~100−300 nm (compactly aggregated, such as at pH 6.8 and 6.5). For all NPs with mixed SAM compositions, the AuNPs were stable at both low and high pH values. The pH-induced aggregation of AuNPs is a result of competition among van der Waals attraction, hydrogen-bonding attraction, electrostatic repulsion, hydration repulsion, and other forces,[66] which are mainly affected by interparticle interactions, as the density of carboxylic charge varies with different pH. Different from the NPs stabilized by

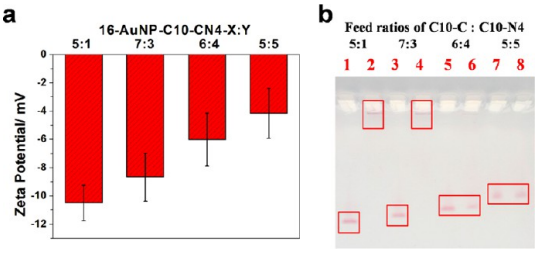

Figure 2. (a) Zeta potential of 16-AuNP-C10-CN4-X:Y at pH 7.4. (b) Gel images of plasma protein adsorption assay. Line 1, line 3, line 5, and line 7: 16-AuNP-C10-CN4-X:Y mixed with phosphate-buffered solution (PB, pH 7.4). Line 2, line 4, line 6, and line 8: AuNPs mixed with platelet-poor plasma.

positive or negative ligand alone with pure electrostatic repulsion, the mixed-charge NPs possess a special zwitterionic characteristic when HS-C10-C ligands were deprotonated, which can be stabilized by hydration repulsion *via* electrostatically induced hydration.[67,68] At high pH, NPs were stabilized in solution due to strong hydration and electrostatic repulsion (all NPs comprising a slightly negative charge, Figure 2a). The strong hydration layer on the mixed-charge NP surface makes them quite stable in solution with high ionic strength, where the electrostatic repulsions are screened (Supporting Information, Figure S2). When the pH decreased to a certain value, the HS-C10-C ligands partially protonated, resulting in attraction of hydrogen bonding, and the hydration of the zwitterionic surface became weak. Once the overall attractions of the van der Waals force and hydrogen bonding surpassed the hydration and electrostatic repulsions, the NPs started to aggregate. As the pH continued to decrease, more and more HS-C10-C ligands were protonated. When the electrostatic repulsions of positive quaternary ammonium surpassed the attraction of the van der Waals force and hydrogen bonding, the NPs underwent dispersion again. A propositional mechanism is presented to better understand the pH-responsive aggregation property (Schemes S1 and S2).

It can be noted that AuNPs modified with equal but opposite ligands in feed ratios demonstrated the most desired pH sensitivity (pH between 7.2 and 7.0) for acidic tumor microenvironment targeting. Another important question is whether the surface composition is the most suitable one for stealth characteristics at physiological pH such as resistance of nonspecific protein adsorption. All AuNPs modified by different C/N4 ratios were demonstrated to well repel protein adsorption in single-protein solution (BSA, 5 mg/mL, Figure S3). Especially, 16-AuNP-C10-CN4-5:5 exhibited the best plasma protein resistance (gel electrophoresis analysis, Figure 2b). It showed that the AuNPs modified with mixed thiols in a more equal ratio have a zeta potential value closer to neutral (*ca.* −4 mV for 16-AuNP-C10-CN4-5:5, Figure 2a). We deduce that the nanoparticles with a surface more resembling a zwitterionic interface of balanced charge possess better nonspecific protein resistance.[62,63,69,70] Unfortunately, the final composition of oppositely charged ligands on the nanoparticles cannot be confirmed at present because of the lack of available analytical techniques for exact quantification. Much effort has been made to modify nanoparticles with zwitterionic ligands, which also demonstrates that the zwitterionic surfaces are closely related to the protein resistance and nonfouling properties of nanoparticles.[34,71−74] Furthermore, the mixed-charge zwitterionic 16-AuNP-C10-CN4-5:5 exhibited excellent long-term stability in biological complex media such as cell culture medium, 100% fetal bovine serum, and 100% human platelet-poor plasma (Figure S4).

As 16-AuNP-C10-CN4-5:5 exhibited a suitable pH transition at tumor extracellular pH and excellent protein resistance, it was selected to prove the hypothesis that controlling aggregation of nanoparticles at tumor pHe can enhance the retention and cellular uptake of small nanoparticles in tumors. Before *in vitro* and *in vivo* studies, the pH sensitivity of 16-AuNP-C10-CN4-5:5 was carefully investigated. The AuNPs aggregated between pH 7.0 and 5.5, while dispersing well at the other pH values (Figure 3a), which was very suitable for targeting the acidic tumor microenvironment. Moreover, they showed a very narrow pH extent for phase transition of only 0.2 unit from pH 7.2 to pH 7.0 (Figure 1b and Figure 3a). The small transition value indicates remarkable pH sensitivity, which will be important for distinguishing the narrow pH difference between normal and tumor tissue.[52,60] Extremely fast pH-induced aggregation was observed (within several seconds) by UV−vis spectra and dynamic light scattering (DLS) measurements (Figure 3b and c). The response time for most pH-sensitive systems achieved by breakage of chemical bonds is on the scale of minutes at least,[48,49,51,58,75] while the time for a mixed-charge system is within a few seconds. Here we attribute the temporal response to the dramatically deionization transition of carboxylic groups in the mixed-charge SAMs, as ionizable groups always render fast and ultrasensitive response to changes in pH value.[76] Besides, the pH-responsive aggregation of these AuNPs was reversible. Even in protein-rich medium, the AuNPs exhibit similar excellent pH sensitivity (Figure 3e and f). Notably, the pH-induced aggregation of the AuNPs could even happen at extremely low concentration and was well reversible in biological media (Figure S5). The good pH sensitivity at a low concentration of NPs indicates the response will still be effective after injected samples are diluted in the blood compartment. It is believed that the rapid and accurate pH-responsive transition of the mixed-charge stabilized nanoparticles will give them a good pH-sensitive performance *in vivo*.

As mentioned above in the introduction, a "stealth" surface of NPs when circulating in blood and normal tissue is a prerequisite for pH-responsive nanoparticles

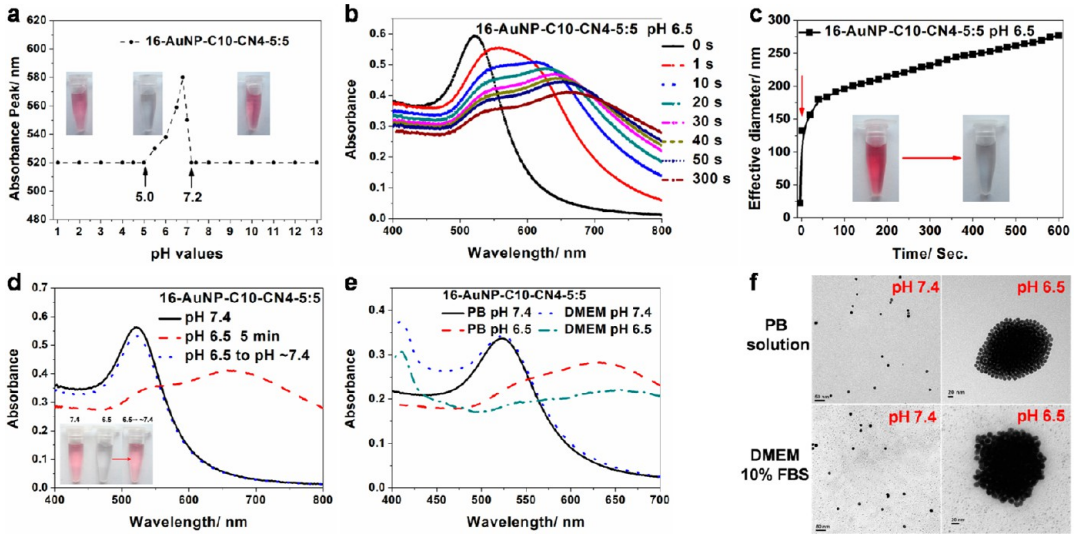

Figure 3. pH sensitivities of mixed-charge AuNPs (16-AuNP-C10-CN4-5:5). (a) Absorbance peak values of AuNPs detected by UV−vis spectrum once added to phosphate-buffered (PB, 50 mM) solution at different pH values. (b) Real-time recording of UV−vis spectra of AuNPs as soon as they are added in PB solution (50 mM, pH 6.5). (c) Real-time recording of DLS results of AuNPs as soon as they are added in the PB solution. Inset is the images of AuNPs when the pH changes from 7.4 (left) to 6.5 (right). (d) UV−vis spectra of AuNPs at pH 7.4 and 6.5 and detected after adjusting the AuNPs from pH 6.5 to *ca*. 7.4 again (inset: digital images of AuNPs for these cases). (e) UV−vis spectra of AuNPs incubated in the PB solution (50 mM) and DMEM culture medium with 10% FBS at pH 7.4 and 6.5. (f) Representative TEM images of AuNPs (scale bar in upper images is 50 nm, and that in lower images is 20 nm).

to target the acidic tumor microenvironment *in vivo*. Before the *in vivo* study, an *in vitro* evaluation of stealth characteristics of AuNPs was carried out. Here the macrophage cell line RAW 264.7 was used as a model of phagocytes in RES.[77] As shown in Figure 4a, the cellular uptake by RAW 264.7 cells at pH 7.4 decreased obviously as the ratio of C/N4 used to modify AuNPs changed from 5:1 to 5:5. Particularly, the uptake of 16-AuNP-C10-CN4-5:5 was even lower than that of traditional PEGylated AuNPs (16-AuNP-PEG2000). This antiphagocytosis tendency of AuNPs is consistent with the protein resistance of NPs as better protein resistance for lower uptake, where 16-AuNP-C10-CN4-5:5 exhibited the best plasma protein resistance (Figure 4a). It promised good steath properties for these AuNPs with a long blood circulation time *in vivo*.

To investigate *in vitro* cell uptake behavior of pH-sensitive AuNPs in a tumor-like acidic environment, the uptake by HepG2 cancer cells was evaluated at both pH 7.4 and 6.5. After cells were incubation with 16-AuNP-C10-CN4-5:5 at pH 6.5 for 12 h, remarkably increased cell uptake was observed, which was about 30-fold higher than that at pH 7.4 (Figure 4b). As a control, there was no observable difference between the two pH conditions for 16-AuNP-PEG2000 or the mixed-charge AuNPs with a pH sensitive range not at pH 6.5 (16-AuNP-C10-CN4-5:1 aggregated at pH from 6.0 to 5.0, Figure 1b). It was found that a notable uptake was observed only after 1 h incubation of 16-AuNP-C10-CN4-5:5 at pH 6.5, which increased dramatically with an increase in incubation time and concentration (Figure 4c and d). TEM analysis further confirmed the obvious internalization of AuNP aggregates in cancer cells when cultured at low pH (Figure 4e and Figure S6), but no detectable uptake by macrophages at normal pH (Figure S7). For other types of cancer cells, such as KB and HeLa cells, similar significant pH-enhanced uptake was also observed (Figure 4f). This demonstrated that the enhanced uptake for pH-induced aggregates seemed to be universal and cell type independent. Albanese *et al*. reported that the cell type might play a significant role in enhancing the uptake of aggregates.[36] The reason for the difference between our system and Albanese's work could be attributed to the different sizes and surfaces of the two systems. Albanese *et al*. fabricated stable aggregates with sizes ranging from 26 to 98 nm and special transferrin coatings. However, in our system, the AuNPs spontaneously aggregated to clusters with sizes up to ~100−300 nm at acidic pH; fast aggregation made the large aggregates sedimentate on the cells subsequently. Besides, the AuNPs with different surfaces will adsorb different serum proteins, which will mediate endocytosis of NPs in different mechanisms. The enhancement of uptake at pH 6.5 is mainly due to the pH-induced surface change and aggregation of AuNPs. Once AuNPs were added to culture medium at pH 6.5, instant aggregation made the large aggregates subsequently sedimentate on the cells, which results in a remarkably high local concentration of NPs on the cell surface and leads to great increase in uptake.[35−37] Furthermore, the AuNPs' surfaces became fouling when aggregated at low pH. These aggregates tend to adsorb serum proteins on their surfaces, which is facile

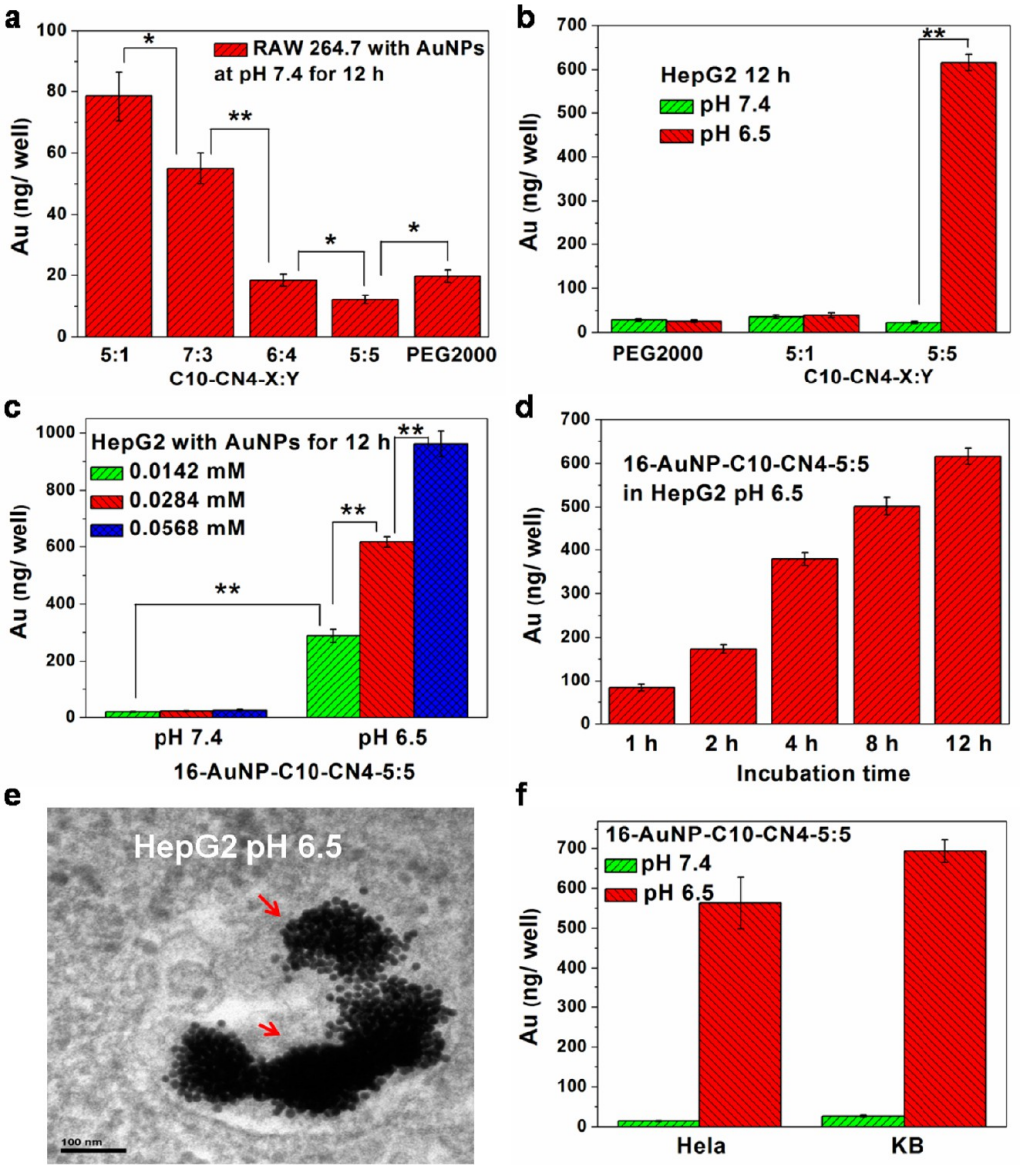

Figure 4. Cell uptake of AuNPs evaluated by ICP-MS and TEM measurements. (a) RAW 264.7 cells after incubation with AuNPs with different surfaces at pH 7.4 for 12 h. (b) HepG2 cells after incubation with AuNPs with different surfaces at pH 7.4 and 6.5 for 12 h. (c) HepG2 cells after incubation with 16-AuNP-C10-CN4-5:5 with different Au concentrations at pH 7.4 and 6.5 for 12 h. (d) HepG2 cells after incubation with AuNPs for different times at pH 6.5. (e) Representative TEM image of a section of HepG2 cells at pH 6.5 after incubation with 16-AuNP-C10-CN4-5:5 for 12 h. (f) KB and HeLa cells after incubation with 16-AuNP-C10-CN4-5:5 for 12 h at pH 7.4 and 6.5. Here except for (c) all concentrations of AuNPs are 0.0284 mM for Au atoms. Error bars represent mean ± SD (n = 3); asterisk indicates significant difference, *p < 0.05 and **p < 0.01.

to mediate endocytosis of NPs. This implies that the pH-responsive zwitterionic nanoparticles can strongly resist phagocytosis by macrophages at normal pH conditions, while the uptake was enhanced greatly by cancer cells once aggregation happens in a tumor-like acidic microenvironment.

After analyzing the inspiring results of the pH-responsive AuNPs *in vitro*, the *in vivo* fate of these zwitterionic AuNPs was studied. The 16-AuNP-C10-CN4-5:5 showed a similar blood circulation time to that of 16-AuNP-PEG2000 after intravenous administration into normal ICR mice (Figure 5a). Nevertheless, a clear difference was observed between the biodistribution of two AuNPs in the main organs (Figure 5b). The accumulations of 16-AuNP-C10-CN4-5:5 in major RES organs, liver and spleen, were lower than those of 16-AuNP-PEG2000. The concentration of Au (μg/g tissue) in the liver and spleen of zwitterionic AuNPs was 55% and 61% for PEGylated AuNPs. Considering the liver is the main high-weight organ in mice, the total RES accumulation of zwitterionic AuNPs could be considered much lower than that of PEGylated AuNPs. It is interesting to note that the blood circulations of 16-AuNP-PEG2000 and 16-AuNP-C10-CN4-5:5 are similar to each other, yet the RES uptakes were quite different from each other. We speculate that the different

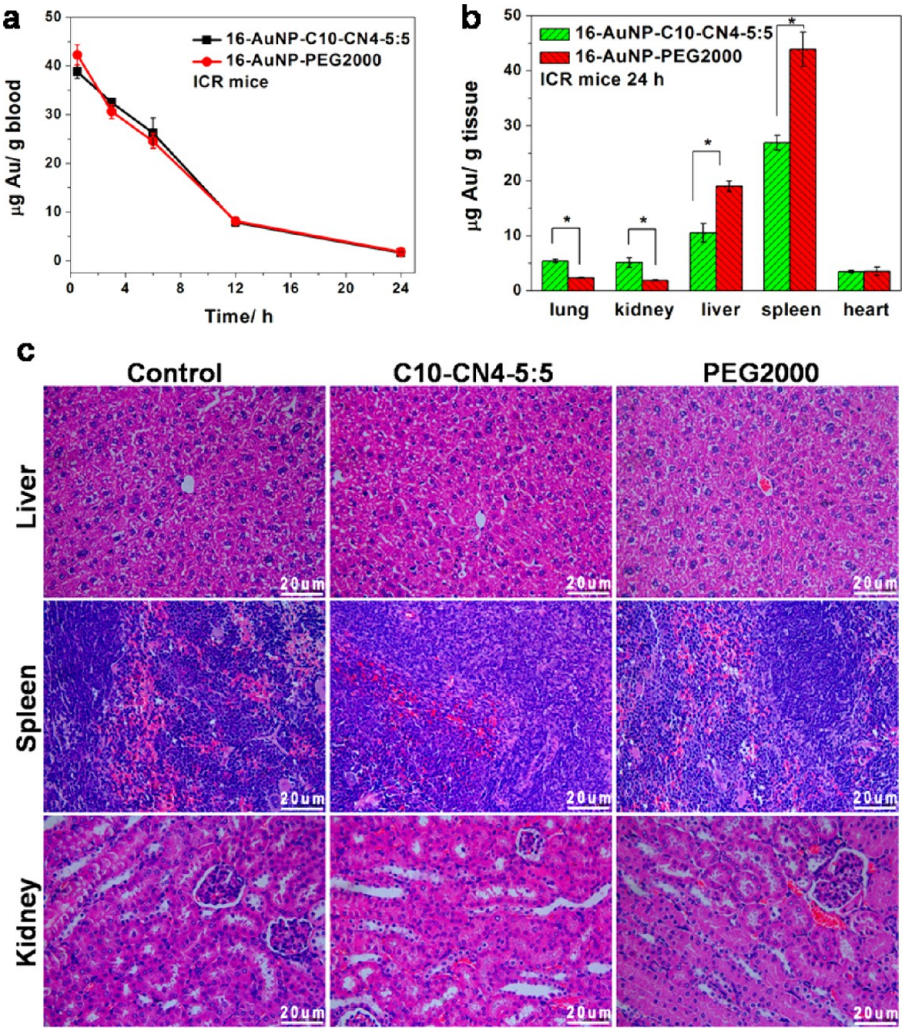

Figure 5. Blood circulation curves (a) and biodistribution (b) of 16-AuNP-C10-CN4-5:5 and 16-AuNP-PEG2000 after intravenously injecting ICR mice. (c) Representative H&E stained images of major organs including liver, spleen, and kidney collected from the control untreated mice and AuNP-injected ICR mice at 24 h postinjection. Error bars represent mean ± SD (n = 3); asterisk indicates significant difference, *p < 0.05). Here each mouse is injected with 100 μg of AuNPs.

phagocytosis of the two AuNPs by phagocytes such as liver Kupffer cells and splenic macrophages is the main reason for their difference in RES uptake. Although lung also contains a significant quantity of macrophages such as alveolar macrophages, the basal membrane in lung can prevent extravasation of nanostructures larger than 10 nm from blood, where the continuous endothelial lining with tight junctions of sizes around 5 nm allows passage of only fluids and small molecules.[78] So there was little chance for the macrophages in lung to phagocytose the AuNPs (core size: 16 nm), which resulted in a much lower accumulation of both AuNPs in lung than that in liver and spleen. An *in vitro* study showed that 16-AuNP-C10-CN4-5:5 had a lower uptake level by the macrophage RAW 264.7 cells than 16-AuNP-PEG2000 (Figure 4a). This indicated that 16-AuNP-C10-CN4-5:5 may have better phagocytic resistance and result in lower RES uptake *in vivo* than 16-AuNP-PEG2000. For blood circulation time, the clearance of NPs from blood is greatly affected by the RES uptake, but it is also affected by the clearance from blood to other non-RES organs. It was observed that the accumulations of 16-AuNP-C10-CN4-5:5 were higher than that of 16-AuNP-PEG2000 in kidney and lung (Figure 5b). Although the 16-AuNP-C10-CN4-5:5 capped by small molecular ligands has a smaller hydrodynamic diameter than the 16-AuNP-PEG2000, this might favor their wide dispersion in organs.[79] The difference may not totally result from the tiny size difference between the two AuNPs (only from the difference in ligand length, ~10 nm). It is more likely that the AuNPs with a zwitterionic surface could distribute in many different organs more rapidly, which needs further investigation. So the similar blood circulation between 16-AuNP-PEG2000 and 16-AuNP-C10-CN4-5:5 could compromise the results of both different RES uptake rate and different rate of NP distribution into non-RES organs. Additionally, no apparent histopathological abnormalities or lesions were observed in liver, spleen, and kidney in the

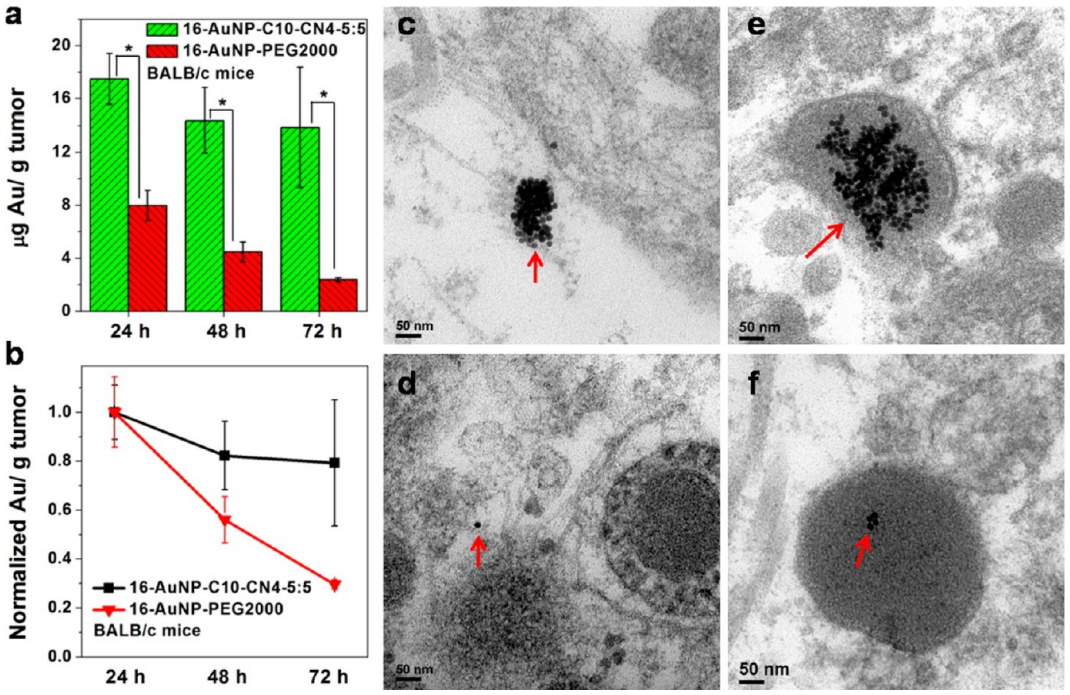

Figure 6. (a) Accumulation of 16-AuNP-C10-CN4-5:5 and 16-AuNP-PEG2000 in KB tumor in BALB/c nude mice at 24, 48, and 72 h postinjection. (b) Tumor uptake normalized at 48 and 72 h postinjection to that at 24 h (error bars represent mean ± SD ($n = 3$); asterisk indicates significant difference, $*p < 0.05$). (c−f) Representative TEM images of sections of KB tumor tissue after injection with AuNPs for 24 h: 16-AuNP-C10-CN4-5:5 located in interstitium (c) and lysosome of tumor cells (e) and 16-AuNP-PEG2000 located in interstitium (d) and lysosome of tumor cells (f); red arrows mark the AuNPs. Each mouse is injected with 100 μg of AuNPs.

16-AuNP-C10-CN4-5:5-treated mice by H&E staining, which showed no noticeable toxic effect of these zwitterionic AuNPs on the major organs of mice at 24 h after NP administration (Figure 5c). *In vitro* evaluation also demonstrated that these zwitterionic gold nanoparticles exhibited no apparent cellular cytotoxicity (Figure S8). Although systematical investigation of the nanotoxicity of these AuNPs by comprehensive analysis for sufficient time is needed before clinic application, the preliminary results indicate ideal biocompatibility of the mixed-charge zwitterionic gold nanoparticles for *in vivo* applications.

Accumulation of nanoparticles in tumors is of critical importance, as it determines the potential impact of a diagnostic or therapeutic effect on the tumor mass.[21,24] The prolonged presence of NPs in tumors is an advantage for many aspects of an NP formulation as bioimaging agent, therapeutic agent, or drug carrier.[80] Tumor retention of AuNPs was evaluated in BALB/c nude mice bearing KB tumors (a representative tumor model with an acidic microenvironment[51]) at three time points of 24, 48, and 72 h postinjection. It was found that the tumor uptake of 16-AuNP-C10-CN4-5:5 was about twice that of 16-AuNP-PEG2000 at 24 h postinjection (Figure 6a). Furthermore, it was observed that the accumulation of 16-AuNP-PEG2000 at 72 h postinjection was further decreased to only ~30% of that at 24 h postinjection. Perrault *et al.* have reported that AuNPs with similar size and surface were not retained in tumors beyond 24 h, which may migrate into surrounding tissues from the tumor.[21] Here, the 16-AuNP-PEG2000 showed a relatively slower clearance rate up to 72 h; the difference may come from the different tumor models used in the two studies. Differently, the retention of 16-AuNP-C10-CN4-5:5 at 72 h postinjection was still ~80% of that at 24 h. The differences between the two AuNPs became more significant as time increased to 72 h, where the accumulation of 16-AuNP-C10-CN4-5:5 was 5−6 times that of 16-AuNP-PEG2000. Normalizing the tumor uptake of AuNPs at different times to that at 24 h, it was clearly observed that the clearance of 16-AuNP-PEG2000 was much faster than that of 16-AuNP-C10-CN4-5:5 (Figure 6b). It was expected that the 16-AuNP-C10-CN4-5:5 aggregated in tumors will sedimentate in the tumor interstitium, then enhance the uptake of nanoparticles by tumor cells due to sedimentation-driven uptake.[35−37] Direct evidence can be provided for this case by TEM analysis of tumor tissue.[81] AuNPs as aggregates located in the interstitial space were observed in TEM sections of tumor after treatment with 16-AuNP-C10-CN4-5:5 (Figure 6c), which supported the argument that pH-responsive aggregation happened in acidic tumor spaces. We also found that the zwitterionic AuNPs were efficiently internalized in tumor cells as aggregates in a similar manner to those internalized in KB cells *in vitro* at pH 6.5 (Figure 6e, Figures S9 and S10). The aggregates were mainly observed in lysosomes,

and no NPs were found directly in the cytosol, mitochondria, and nucleus, suggesting that the AuNPs enter the cells predominantly through the endocytic pathway.[36,82] Differently, the PEGylated AuNPs remain individual in the interstitial space within the tumor as single particles (Figure 6d). This clearly demonstrates the difference in aggregation state of the two types of AuNPs. Moreover, much fewer nonresponsive PEGylated AuNPs were observed in tumor tissue, and only a few small aggregates of 16-AuNP-PEG2000 in lysosomes of tumor cells were found, as their endocytosis was prevented by PEG this time (Figure 6f). The size of 16-AuNP-PEG2000 aggregates in cells was much smaller than that of 16-AuNP-C10-CN4-5:5, which could be formed during the endocytosis process. This also partially demonstrates the different aggregation states between the two AuNPs in tumor tissue. Silver enhancement of tumor histological sections also showed that, compared to the case of PEGylated AuNPs, much more zwitterionic AuNPs look like aggregates localized in the tumor (Figure S11).

As the blood circulation curves of the two AuNPs were very similar to each other, they were expected to have similar chances to enter the tumor *via* leaky vasculature. In fact, tumor accumulation is a function of both the rate of extravasation from the blood to the tumor space and the rate of clearance out of the tumor. Particles that enter the tumor through leaky vasculature may be carried by convection past the tumor periphery and into the surrounding tissue, where they are likely to be cleared.[21] Perrault *et al*. demonstrated that tumor accumulation of particles in the 20 nm range depends on effects of both size and half-life.[21] Therefore, the tumor accumulation of 16-AuNP-PEG2000 would be a combined result of AuNPs extravasated from the blood with high NP concentration to the tumor space and those cleared from the tumor to periphery tissues at a high rate at the same time. However, for the pH-responsive 16-AuNP-C10-CN4-5:5, once arriving at the tumor tissue, they aggregated quickly, stimulated by the acidic tumor microenvironment, which restricts their migration into surrounding tissues owing to the formed aggregates with large size, which were firmly trapped in the tumor extracellular matrix. What's more, the enhanced uptake of aggregates will also favor the retention of the zwitterionic AuNPs, but the PEGylation of AuNPs is not favorable for cell uptake. So even though the 16-AuNP-C10-CN4-5:5 and 16-AuNP-PEG2000 have similar blood circulation times, which means they had a similar chance to extravasate into the tumor, the different retention and cell uptake abilities result in quite different tumor accumulation of the two AuNPs.

In addition, considering the NPs with small size will have the advantage of deep penetration into the tumor, the remaining question is whether the aggregation-responsive AuNPs still have a chance to penetrate deep into the tumor. For the pH-responsive 16-AuNP-C10-CN4-5:5 with small size before aggregation, the penetration problem depends on which part of the tumor is more acidic. In the site with pH > 7.0, the AuNPs could exist as small single particles, which may migrate into the deep interstitial space.[21] When arriving at the site with pH < 7.0, they quickly aggregate, resulting in large sizes, which will be trapped right in place. The outer region of the tumor tissue near the blood supply is less hypoxic and less acidic, and the inner region of the tumor far away from the blood supply is more hypoxic and more acidic.[10,43] AuNPs that look like aggregates localized perivascularly or migrated far into the interstitial space in the tumor were observed in the silver-enhanced tumor histological sections (Figure S11). This indicated that the pH-responsive AuNP system might also penetrate deeply into tumors.

Although aggregation of nanoparticles is usually considered a serious problem in nanobiotechnology, a design of controllable aggregation can be beneficial, similar to "turning lemons into lemonade".[83,84] It was noted that pH-induced aggregation shifts the absorption band of AuNPs to the NIR wavelength (Figure 3), which can be applied for NIR photothermal therapies with deep tissue penetrations.[58] As cancer cells are more sensitive to temperature (usually >42 °C) than normal cells, the heat generated by AuNPs attached on or internalized in cells can effectively damage cancer cells. HepG2 cells incubated with PEG and mixed charge modified AuNPs at pH 7.4 and pH 6.5 were irradiated under the same NIR laser beam using a continuous wave (CW) diode laser of 808 nm. Serious damage to cells was observed in the test group with 16-AuNP-C10-CN4-5:5 at pH 6.5 (Figure 7d), but was not observed in the test groups with 16-AuNP-C10-CN4-5:5 at pH 7.4 (Figure 7b), 16-AuNP-PEG2000 at pH 7.4 (Figure 7a), and 16-AuNP-PEG2000 at pH 6.5 (Figure 7c). When cells were cultured at pH 6.5 *in vitro*, the acidic pH will slightly affect the cell viability, but the aggregation of 16-AuNP-C10-CN4-5:5 at this pH did not induce more toxicity to the cells (Figure S12). So here, the serious damage to cells in the test group with 16-AuNP-C10-CN4-5:5 at pH 6.5 irradiated by the NIR laser was a result of photothermal ablation of the cells assisted by AuNP aggregates. Kim *et al*. have reported a "smart" gold nanoparticle that aggregates in acidic intracellular pH by its hydrolysis-susceptible surface for photothermal cancer therapy.[58] Differently, the pH-induced aggregation in this system has a much faster and more ultrasensitive transition between normal tissues (7.2−7.4) and most solid tumors (6.0−7.0). Moreover, the mixed-charge 16-AuNP-C10-CN4-5:5 with zwitterionic surfaces at pH 7.4 have good stealth properties, which endow them with a long blood half-life and effective tumor accumulation after intravenous injection. We further preliminarily

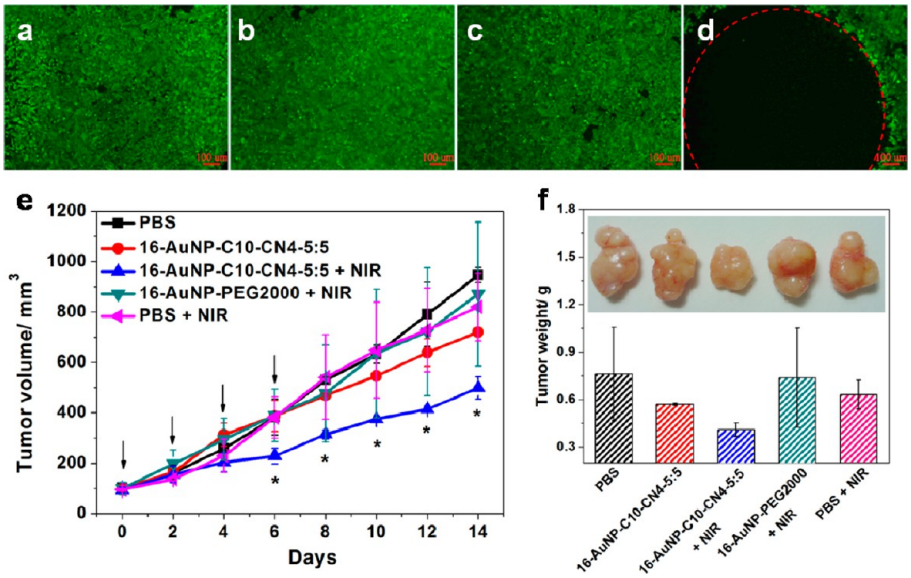

Figure 7. (a–d) Cell viability assessed *via* fluorescein diacetate (FDA) staining. After treatment with NPs for 1 h, cells were irradiated with an 808 nm laser of 400 mW for 1 min: (a–c) no dead cells in the test group with 16-AuNP-PEG2000 at pH 7.4 (a) and pH 6.5 (c) and 16-AuNP-C10-CN4-5:5 at pH 7.4 (b); (d) cell death and disappearance within the spot for 16-AuNP-C10-CN4-5:5 at pH 6.5. (e) Tumor size at different time points postirradiation of mice treated with 16-AuNP-C10-CN4-5:5 plus NIR laser and other applied conditions. Black arrows indicate irradiation with an 808 nm laser of 800 mW for 1 min. Error bars represent mean ± SD (n = 3); asterisk indicates significant difference, *p < 0.05 for 16-AuNP-C10-CN4-5:5 plus NIR laser treated group *versus* all other groups. (f) Tumor weight after 2 weeks postirradiation of mice treated with 16-AuNP-C10-CN4-5:5 plus NIR laser and other applied conditions. Error bars represent mean ± SD (n = 3); p = 0.11, 0.015, 0.15, and 0.032 for 16-AuNP-C10-CN4-5:5 + NIR treated group *versus* PBS treated group, 16-AuNP-C10-CN4-5:5 treated group, 16-AuNP-PEG2000 + NIR treated group, and PBS + NIR treated groups, respectively. Insets are representative images of tumors after corresponding treatments.

evaluated the possibility of NIR photothermal ablation of tumors using this kind of pH-responsive AuNPs *in vivo*. After a single injection of AuNPs, the tumors on mice were irradiated with a mild NIR laser at 808 nm. As shown in Figure 7e, the tumor volume of 16-AuNP-C10-CN4-5:5 plus NIR treated mice increased significantly slower than those of the 16-AuNP-PEG2000 plus NIR treated group and groups treated with other control conditions from the sixth day after the first NIR treatment. The tumor weight after 2 weeks postirradiation of mice treated with 16-AuNP-C10-CN4-5:5 plus NIR laser was also lower than those of mice treated with all other applied conditions (Figure 7f). This demonstrated the 16-AuNP-C10-CN4-5:5 plus NIR laser have possible tumor inhibition ability, which deserves further preclinical and even clinical studies.

CONCLUSION

In summary, we demonstrate that gold nanoparticles with fast, ultrasensitive, and reversible pH sensitivity can be simply prepared by surface modification with mixed-charge zwitterionic SAMs. The zwitterionic AuNPs are stable with a stealth surface at normal pH during circulation but quickly aggregate in the acidic extracellular pH of solid tumors once arriving in the tumor. The mixed-charge zwitterionic strategy can further be used to easily fabricate other functional nanoparticles with stealth properties and desirable pH sensitivity simultaneously. The total accumulation, retention, and cell uptake of the pH-responsive AuNPs in tumors are significantly enhanced by the pH-induced aggregation effect compared with that of nonsensitive PEGylated AuNPs. A preliminary photothermal tumor ablation evaluation suggests that the aggregation of AuNPs can be applied in cancer NIR photothermal therapy. Considering that the microenvironment in tumors is always different from that in normal tissue, controlling the aggregation of NPs responding to the tumor environment, such as low pH, low O_2, or matrix metalloproteinase enzymatic activity, can serve as a universal strategy to enhance retention and cell uptake of inorganic NPs in tumors and improve the performance of NPs used in cancer diagnosis and treatment.

EXPERIMENTAL SECTION

Synthesis of Thiol-Protected AuNPs. Citrate-capped AuNPs with a diameter of *ca.* 16 nm and thiol-modified AuNPs were prepared according to previous reports.[33] A series of mixed-charge SAMs protected AuNPs with different surface charges were prepared by adding the same total concentration of thiols with different molar ratios of HS-C10-C to HS-C10-N4 to the same amount of citrate-coated 16 nm Au-NPs. Here, we refer to these Au-NPs as 16-AuNP-C10-CN4-X:Y (X:Y means the feed ratios of HS-C10-C to HS-C10-N4). The HS-PEG2000-modified AuNPs were named

16-AuNP-PEG2000 as described previously.[33] Taking 16-AuNP-C10-CN4-5:5 as an example to describe the synthesis routes, briefly, a mixed thiol aqueous solution (25 mM, 1 mL) that contained a 5:5 molar ratio of HS-C10-C and HS-C10-N4 was added into the original citrate-coated 16 nm AuNP solution (10 mL). The pH of the solution was adjusted to pH ~9 with 1 M NaOH, as HS-C10-C has a better solubility in alkaline conditions, and it is also helpful for keeping the AuNPs stable through the ligand exchange reaction. After stirring at room temperature for 24 h, the modified AuNPs were purified by centrifuging twice at 16 000 rpm for 10 min. Then the AuNPs were redispersed in water, and drops of phosphate buffer solution (10 mM PB, pH 7.4) were added to adjust the pH to ~7.4, making a dispersed AuNP solution. Similarly, the Au-NPs protected by different ratios of mixed-charge thiols and other thiols were prepared in the same way.

Measurement of pH Sensitivity of AuNPs. To determine the AuNPs' sensitivity with respect to pH, 10 μL of purified AuNPs was added to 190 μL of PB (50 mM) solutions with different pHs. For the pH sensitivity of AuNPs in biological media, AuNPs were added to cell culture media with 10% fetal bovine serum (FBS) at different pHs. The stability of gold nanoparticles was detected by color change observation, UV−vis spectrum, DLS, and TEM measurements.

AuNPs Interaction with BSA and Plasma. The interaction of AuNPs with BSA or plasma was measured by gel electrophoresis. The experiments were done by mixing 5 μL of AuNPs with 5 μL of 10 mg/mL BSA or 40% human platelet-poor plasma. After incubation at room temperature for 10 min, the mixture was loaded on a 1% agarose gel buffered with 0.5× TBE (Tris-borate-EDTA, pH 7.4). Gel electrophoresis was also run in 0.5× TBE buffer at 120 V constant voltage for 15 min. Gel shift bands were directly recorded by digital camera.

Cell Culture. RAW 264.7 cells, HepG2 cells, and HeLa cells were cultured with regular growth medium consisting of high-glucose DMEM, and KB cells were cultured with RPMI 1640. All cell growth media were supplemented with 10% FBS, 100 U/mL penicillin, and 100 mg/mL streptomycin and cultured at 37 °C in a 5% CO_2 humidified environment. Cell culture media with different pHs were prepared in 25 mM HEPES and adjusted by NaOH to a final pH value.

Cellular Uptake of AuNPs. Cellular uptake of the AuNPs was determined by ICP-MS quantitatively. To determine the AuNP uptake amount quantitatively, the cells were seeded on a 24-well plate at a certain density (1×10^5 cells per well for HepG2, KB, and HeLa and 2×10^5 cells per well for RAW 264.7, which volume is much smaller than that of HepG2, KB, and HeLa). After culturing for 24 h, the medium was replaced with fresh medium at pH 7.4 or 6.5, and then the cells were incubated with AuNPs of varying concentration for 12 h or other time intervals. At a determined time, the cells were washed five times with PBS and then treated with aqua regia (HCl/HNO_3 = 1:3, volume ratio) for 2 h. The treated solution was diluted 20 times to measure Au concentration by ICP-MS (Thermo Elemental Corporation of USA, X Series II).

Internalization of AuNPs Detected by TEM Analysis. For TEM cell sections analysis, the cells were seeded on a six-well plate at a certain density (5×10^5 cells per well for HepG2 and KB, 1×10^6 cells per well for RAW 264.7) and cultured for 24 h. After culturing for 24 h, the medium was replaced with fresh medium at pH 7.4 or 6.5, and then the cells were incubated with AuNPs with a Au atomic concentration of about 0.0284 mM for 12 h. At a determined time, the cells were washed five times with PBS and trypsizined, centrifuged, and then fixed with 2.5% glutaraldehyde. After 2 h fixation at 4 °C, the samples were washed with phosphate-buffered saline (0.1 M, pH = 7.0) three times. Then the samples were fixed with 1% perosmic oxide for 2 h at 4 °C. After being washed by water, the samples were dehydrated in an alcohol series, embedded, and sliced with a thickness of 50 to 70 nm.

NIR Photothermal Assay *in Vitro*. HepG2 cells were cultivated as above to near 100% confluence. After treating with 0.0284 mM AuNPs for 1 h at pH 7.4 and pH 6.5, respectively, the medium was carefully removed and the cells were irradiated using an NIR laser with a 1 mm focused spot size. The efficiency of photoinduced cancer cell thermal ablation was investigated with various power densities of the CW laser at 808 nm and different irradiation times. The cell viability was confirmed by staining the cells with FDA. The live cells can manufacture fluorescein from FDA by esterase inside cells, while the dead cells cannot. The diode continuous wave laser with a wavelength of 808 nm was from Hi-Tech Optoelectronics Co., Ltd.

Animals. Animal experiments were performed according to the Guidelines for Animal Care and Use Committee, Zhejiang University. Healthy male ICR mice and male BALB/c mice were purchased from the animal center of Zhejiang Academy of Medical Sciences.

Blood Circulation and Biodistribution. Blood circulation and biodistribution of gold nanoparticles were first evaluated in healthy male ICR mice (20−24 g). Nanoparticles in 0.2 mL of PBS with 100 μg of Au were injected *via* the tail vein in each mouse. Blood circulation analysis was performed by measuring the remaining gold content from blood taken after injection at different times. Biodistribution analysis was performed by measuring the gold content in different tissues 24 h after injection. Examined tissues include liver, kidneys, spleen, heart, and lung. The gold content was analyzed by ICP-MS.

Histology. For histology, major organs (liver, kidneys, and spleen) were harvested from mice 24 h after injection. Organs were fixed in 3.7% neutral buffered formalin, processed routinely into paraffin, sectioned into ~4 μm, and stained with hematoxylin and eosin (H&E). The histology was performed in a blinded fashion by professional personnel in the medical college of Zhejiang University. The samples were examined by microscope (Olympus BX61 inverted microscope) in bright field.

Tumor Accumulation and Cell Internalization. KB cells (2×10^6) in 0.1 mL of PBS were injected subcutaneously into the right rear flank area of male nude BALB/c mice of weight 16 to 18 g. Tumors were allowed to grow to ~100 mm^3 before experimentation. Nanoparticles in 0.2 mL of PBS with 100 μg of Au were injected *via* the tail vein in each mouse. Tumors were collected for measuring their Au content by ICP-MS at 24, 48, and 72 h postinjection. Tumors at 24 h were also collected for cell internalization of AuNP analysis by TEM sections and histological silver enhancement analysis.

ICP-MS Measurement. Organs and tumors were washed with PBS buffer and lyophilized for 1 day. Blood was lyophilized directly. The dried tissues and blood were mashed and dissolved in aqua regia (2 mL for liver and 1 mL for all others) for 1 day. Tissue debris was removed by centrifugation at 10 000 rpm for 5 min. After dilution, the Au content was detected by ICP-MS.

Transmission Electron Microscopy. Tumors were first fixed in 2.5% glutaraldehyde (in 0.1 M phosphate buffer, pH 7.0). Then the samples were fixed with 1% perosmic oxide for 2 h at 4 °C. After being washed in water, the samples were dehydrated in an alcohol series, embedded, and sliced with a thickness of 50 to 70 nm.

Histological Silver Enhancement. For silver enhancement, the tissue sections were dewaxed with xylene, washed consecutively with 100%, 90%, 70%, and 30% ethanol, and immersed in a silver enhancement solution for 5 min, which is composed of equal amounts of solutions A and B from the Silver Enhancer Kit (Sigma-Aldrich). After rinsing, the tissue sections were fixed with 2.5% sodium thiosulfate for 3 min, washed with DI water, and then stained with hematoxylin and eosin (H&E). The samples were examined by microscope (Olympus IX81 inverted microscope) in bright field.

NIR Photothermal Assay *in Vivo*. KB cells (2×10^6) in 0.1 mL of PBS were injected subcutaneously into the right rear flank area of male nude BALB/c mice of weight 16 to 18 g. Tumors were allowed to grow to ~100 mm^3 before experimentation. Nanoparticles in 0.2 mL of PBS with 100 μg of Au or pure PBS without AuNPs as control were injected *via* the tail vein in each mouse. After 24 h, the tumors were irradiated using a CW laser at 808 nm with a ~6 mm focused spot size and a power density of 800 mW. The tumors were irradiated every two days up to the sixth day after the first treatment. Tumor dimensions (length and width) were measured using a caliper. The tumor volume was calculated as length × $width^2/2$ (mm^3). The tumor volume

of all treated groups was recorded every two days, the mice were sacrificed after 2 weeks postirradiation, and the tumors were weighed. The diode continuous wave laser (MDL-N-808 nm) with a wavelength of 808 nm was from Changchun New Industries Optoelectronics Tech. Co., Ltd.

Statistical Analysis. All the experiments were repeated at least three times, and the data are presented as means ± standard deviation (SD). The statistical significance ($p < 0.05$) was evaluated by Student'S *t* test when only two groups were compared. One-way analysis of variance (ANOVA) with Tukey's test was used for multiple comparisons. In all tests, the statistical significance was set at $p < 0.05$.

Conflict of Interest: The authors declare no competing financial interest.

Acknowledgment. Financial support from the National Science Fund for Distinguished Young Scholars (51025312), the National Basic Research Program of China (2011CB606203), NSFC-50830106 and 21174126, Open Project of State Key Laboratory of Supramolecular Structure and Materials (SKLSSM 201204), and Research Fund for the Doctoral Program of Higher Education of China (20110101110037, 20110101120049, and 20120101130013) is gratefully acknowledged. We would like to thank Guping Tang and Jun Zhou for animal experiments, Ying Xu and Hua Wang for TEM, and Zigang Xu for ICP-MS.

Supporting Information Available: Figures S1 to S12. More experimental details. This material is available free of charge *via* the Internet at http://pubs.acs.org.

REFERENCES AND NOTES

1. Gao, X. H.; Cui, Y. Y.; Levenson, R. M.; Chung, L. W. K.; Nie, S. M. *In Vivo* Cancer Targeting and Imaging with Semiconductor Quantum Dots. *Nat. Biotechnol.* **2004**, *22*, 969–976.
2. Brigger, I.; Dubernet, C.; Couvreur, P. Nanoparticles in Cancer Therapy and Diagnosis. *Adv. Drug Delivery Rev.* **2002**, *54*, 631–651.
3. Ferrari, M. Cancer Nanotechnology: Opportunities and Challenges. *Nat. Rev. Cancer* **2005**, *5*, 161–171.
4. Giljohann, D. A.; Seferos, D. S.; Daniel, W. L.; Massich, M. D.; Patel, P. C.; Mirkin, C. A. Gold Nanoparticles for Biology and Medicine. *Angew. Chem., Int. Ed.* **2010**, *49*, 3280–3294.
5. Cobley, C. M.; Chen, J. Y.; Cho, E. C.; Wang, L. V.; Xia, Y. N. Gold Nanostructures: A Class of Multifunctional Materials for Biomedical Applications. *Chem. Soc. Rev.* **2011**, *40*, 44–56.
6. Graham, B.; Barreto, J. A.; O'Malley, W.; Kubeil, M.; Stephan, H.; Spiccia, L. Nanomaterials: Applications in Cancer Imaging and Therapy. *Adv. Mater.* **2011**, *23*, H18–H40.
7. Qiao, R.; Zeng, J.; Jia, Q.; Du, J.; Shen, L.; Gao, M. Magnetic Iron Oxide Nanoparticle-an Important Footstone towards MR Molecular Imaging of Tumor. *Acta Phys.-Chim. Sin.* **2012**, *28*, 993–1011.
8. Saha, K.; Agasti, S. S.; Kim, C.; Li, X.; Rotello, V. M. Gold Nanoparticles in Chemical and Biological Sensing. *Chem. Rev.* **2012**, *112*, 2739–2779.
9. Duncan, R.; Gaspar, R. Nanomedicine(s) under the Microscope. *Mol. Pharmaceut.* **2011**, *8*, 2101–2141.
10. Jain, R. K.; Stylianopoulos, T. Delivering Nanomedicine to Solid Tumors. *Nat. Rev. Clin. Oncol.* **2010**, *7*, 653–664.
11. Stark, W. J. Nanoparticles in Biological Systems. *Angew. Chem., Int. Ed.* **2011**, *50*, 1242–1258.
12. Maeda, H.; Wu, J.; Sawa, T.; Matsumura, Y.; Hori, K. Tumor Vascular Permeability and the EPR Effect in Macromolecular Therapeutics: A Review. *J. Controlled Release* **2000**, *65*, 271–284.
13. Duan, X.; Li, Y. Physicochemical Characteristics of Nanoparticles Affect Circulation, Biodistribution, Cellular Internalization, and Trafficking. *Small* **2013**, *9*, 1521–1532.
14. Albanese, A.; Tang, P. S.; Chan, W. C. W. The Effect of Nanoparticle Size, Shape, and Surface Chemistry on Biological Systems. *Annu. Rev. Biomed. Eng.* **2012**, *14*, 1–16.
15. Moghimi, S. M.; Hunter, A. C.; Murray, J. C. Long-Circulating and Target-Specific Nanoparticles: Theory to Practice. *Pharmacol. Rev.* **2001**, *53*, 283–318.
16. Dobrovolskaia, M. A.; Aggarwal, P.; Hall, J. B.; McNeil, S. E. Preclinical Studies to Understand Nanoparticle Interaction with the Immune System and Its Potential Effects on Nanoparticle Biodistribution. *Mol. Pharmaceut.* **2008**, *5*, 487–495.
17. Li, S.-D.; Huang, L. Pharmacokinetics and Biodistribution of Nanoparticles. *Mol. Pharmaceut.* **2008**, *5*, 496–504.
18. Gref, R.; Domb, A.; Quellec, P.; Blunk, T.; Muller, R. H.; Verbavatz, J. M.; Langer, R. The Controlled Intravenous Delivery of Drugs Using PEG-Coated Sterically Stabilized Nanospheres. *Adv. Drug Delivery Rev.* **1995**, *16*, 215–233.
19. Storm, G.; Belliot, S. O.; Daemen, T.; Lasic, D. D. Surface Modification of Nanoparticles to Oppose Uptake by the Mononuclear Phagocyte System. *Adv. Drug Delivery Rev.* **1995**, *17*, 31–48.
20. Niidome, T.; Yamagata, M.; Okamoto, Y.; Akiyama, Y.; Takahashi, H.; Kawano, T.; Katayama, Y.; Niidome, Y. PEG-Modified Gold Nanorods with a Stealth Character for *in Vivo* Applications. *J. Controlled Release* **2006**, *114*, 343–347.
21. Perrault, S. D.; Walkey, C.; Jennings, T.; Fischer, H. C.; Chan, W. C. W. Mediating Tumor Targeting Efficiency of Nanoparticles through Design. *Nano Lett.* **2009**, *9*, 1909–1915.
22. Larsen, E. K.; Nielsen, T.; Wittenborn, T.; Birkedal, H.; Vorup-Jensen, T.; Jakobsen, M. H.; Østergaard, L.; Horsman, M. R.; Besenbacher, F.; Howard, K. A. Size-Dependent Accumulation of PEGylated Silane-Coated Magnetic Iron Oxide Nanoparticles in Murine Tumors. *ACS Nano* **2009**, *3*, 1947–1951.
23. Han, H. S.; Martin, J. D.; Lee, J.; Harris, D. K.; Fukumura, D.; Jain, R. K.; Bawendi, M. Spatial Charge Configuration Regulates Nanoparticle Transport and Binding Behavior *in Vivo*. *Angew. Chem., Int. Ed.* **2013**, *52*, 1414–1419.
24. Idris, N. M.; Gnanasammandhan, M. K.; Zhang, J.; Ho, P. C.; Mahendran, R.; Zhang, Y. *In Vivo* Photodynamic Therapy Using Upconversion Nanoparticles as Remote-Controlled Nanotransducers. *Nat. Med.* **2012**, *18*, 1580–1586.
25. Arvizo, R. R.; Miranda, O. R.; Moyano, D. F.; Walden, C. A.; Giri, K.; Bhattacharya, R.; Robertson, J. D.; Rotello, V. M.; Reid, J. M.; Mukherjee, P. Modulating Pharmacokinetics, Tumor Uptake and Biodistribution by Engineered Nanoparticles. *Plos One* **2011**, *6*, e24374.
26. Bonitatibus, P. J., Jr.; Torres, A. S.; Kandapallil, B.; Lee, B. D.; Goddard, G. D.; Colborn, R. E.; Marino, M. E. Preclinical Assessment of a Zwitterionic Tantalum Oxide Nanoparticle X-Ray Contrast Agent. *ACS Nano* **2012**, *6*, 6650–6658.
27. Li, A.; Luehmann, H. P.; Sun, G.; Samarajeewa, S.; Zou, J.; Zhang, S.; Zhang, F.; Welch, M. J.; Liu, Y.; Wooley, K. L. Synthesis and *In Vivo* Pharmacokinetic Evaluation of Degradable Shell Cross-Linked Polymer Nanoparticles with Poly(carboxybetaine) *versus* Poly(ethylene glycol) Surface-Grafted Coatings. *ACS Nano* **2012**, *6*, 8970–8982.
28. Zhang, L.; Cao, Z.; Li, Y.; Ella-Menye, J. R.; Bai, T.; Jiang, S. Softer Zwitterionic Nanogels for Longer Circulation and Lower Splenic Accumulation. *ACS Nano* **2012**, *6*, 6681–6686.
29. Wei, H.; Bruns, O. T.; Chen, O.; Bawendi, M. G. Compact Zwitterion-Coated Iron Oxide Nanoparticles for *in Vitro* and *in Vivo* Imaging. *Integr. Biol.* **2013**, *5*, 108–114.
30. Ohyanagi, T.; Nagahori, N.; Shimawaki, K.; Hinou, H.; Yamashita, T.; Sasaki, A.; Jin, T.; Iwanaga, T.; Kinjo, M.; Nishimura, S. I. Importance of Sialic Acid Residues Illuminated by Live Animal Imaging Using Phosphorylcholine Self-Assembled Monolayer-Coated Quantum Dots. *J. Am. Chem. Soc.* **2011**, *133*, 12507–12517.
31. Gong, Y.; Winnik, F. M. Strategies in Biomimetic Surface Engineering of Nanoparticles for Biomedical Applications. *Nanoscale* **2012**, *4*, 360–368.
32. Perrault, S. D.; Chan, W. C. W. Synthesis and Surface Modification of Highly Monodispersed, Spherical Gold Nanoparticles of 50−200 nm. *J. Am. Chem. Soc.* **2009**, *131*, 17042–17043.
33. Liu, X. S.; Huang, H. Y.; Jin, Q.; Ji, J. Mixed Charged Zwitterionic Self-Assembled Monolayers as a Facile Way to Stabilize Large Gold Nanoparticles. *Langmuir* **2011**, *27*, 5242–5251.

34. Jin, Q.; Xu, J. P.; Ji, J.; Shen, J. C. Zwitterionic Phosphorylcholine as a Better Ligand for Stabilizing Large Biocompatible Gold Nanoparticles. *Chem. Commun.* **2008**, 3058–3060.
35. Limbach, L. K.; Li, Y.; Robert, N.; Brunner, T. J.; Hintermann, M. A.; Muller, M.; Gunther, D.; Stark, W. J. Oxide Nanoparticle Uptake in Human Lung Fibroblasts: Effects of Particle Size, Agglomeration, and Diffusion at Low Concentrations. *Environ. Sci. Technol.* **2005**, *39*, 9370–9376.
36. Albanese, A.; Chan, W. C. Effect of Gold Nanoparticle Aggregation on Cell Uptake and Toxicity. *ACS Nano* **2011**, *5*, 5478–5489.
37. Cho, E. C.; Zhang, Q.; Xia, Y. The Effect of Sedimentation and Diffusion on Cellular Uptake of Gold Nanoparticles. *Nat. Nanotechnol.* **2011**, *6*, 385–391.
38. Ganta, S.; Devalapally, H.; Shahiwala, A.; Amiji, M. A Review of Stimuli-Responsive Nanocarriers for Drug and Gene Delivery. *J. Controlled Release* **2008**, *126*, 187–204.
39. Gao, W. W.; Chan, J. M. C.; Farokhzad, O. C. pH-Responsive Nanoparticles for Drug Delivery. *Mol. Pharmaceut.* **2010**, *7*, 1913–1920.
40. Warburg, O. *The Metabolism of Tumours*; Constable Press: London. 1930.
41. Gatenby, R. A.; Gillies, R. J. Why Do Cancers Have High Aerobic Glycolysis? *Nat. Rev. Cancer* **2004**, *4*, 891–899.
42. Tannock, I. F.; Rotin, D. Acid pH in Tumors and Its Potential for Therapeutic Exploitation. *Cancer Res.* **1989**, *49*, 4373–4384.
43. Helmlinger, G.; Yuan, F.; Dellian, M.; Jain, R. K. Interstitial pH and pO2 Gradients in Solid Tumors *in Vivo*: High-Resolution Measurements Reveal a Lack of Correlation. *Nat. Med.* **1997**, *3*, 177–182.
44. Cardone, R. A.; Stephan, V. C.; Reshkin, J. The Role of Disturbed pH Dynamics and the Na^+/H^+ Exchanger in Metastasis. *Nat. Rev. Cancer* **2005**, *5*, 786–795.
45. Zhang, L.; Guo, R.; Yang, M.; Jiang, X.; Liu, B. Thermo and pH Dual-Responsive Nanoparticles for Anti-Cancer Drug Delivery. *Adv. Mater.* **2007**, *19*, 2988–2992.
46. Bae, Y. H.; Lee, E. S.; Gao, Z. G. Recent Progress in Tumor pH Targeting Nanotechnology. *J. Controlled Release* **2008**, *132*, 164–170.
47. Gu, J. X.; Cheng, W. P.; Liu, J. G.; Lo, S. Y.; Smith, D.; Qu, X. Z.; Yang, Z. Z. pH-Triggered Reversible "Stealth" Polycationic Micelles. *Biomacromolecules* **2008**, *9*, 255–262.
48. Du, J. Z.; Sun, T. M.; Song, W. J.; Wu, J.; Wang, J. A Tumor-Acidity-Activated Charge-Conversional Nanogel as an Intelligent Vehicle for Promoted Tumoral-Cell Uptake and Drug Delivery. *Angew. Chem., Int. Ed.* **2010**, *49*, 3621–3626.
49. Yuan, Y. Y.; Mao, C. Q.; Du, X. J.; Du, J. Z.; Wang, F.; Wang, J. Surface Charge Switchable Nanoparticles Based on Zwitterionic Polymer for Enhanced Drug Delivery to Tumor. *Adv. Mater.* **2012**, *24*, 5476–5480.
50. Gao, G. H.; Im, G. H.; Kim, M. S.; Lee, J. W.; Yang, J.; Jeon, H.; Lee, J. H.; Lee, D. S. Magnetite-Nanoparticle-Encapsulated pH-Responsive Polymeric Micelle as an MRI Probe for Detecting Acidic Pathologic Areas. *Small* **2010**, *6*, 1201–1204.
51. Poon, Z. Y.; Chang, D. S.; Zhao, X. Y.; Hammond, P. T. Layer-by-Layer Nanoparticles with a pH-Sheddable Layer for *in Vivo* Targeting of Tumor Hypoxia. *ACS Nano* **2011**, *5*, 4284–4292.
52. Callahan, D. J.; Liu, W.; Li, X.; Dreher, M. R.; Hassouneh, W.; Kim, M.; Marszalek, P.; Chilkoti, A. Triple Stimulus-Responsive Polypeptide Nanoparticles That Enhance Intratumoral Spatial Distribution. *Nano Lett.* **2012**, *12*, 2165–2170.
53. Mandal, S.; Gole, A.; Lala, N.; Gonnade, R.; Ganvir, V.; Sastry, M. Studies on the Reversible Aggregation of Cysteine-Capped Colloidal Silver Particles Interconnected *via* Hydrogen Bonds. *Langmuir* **2001**, *17*, 6262–6268.
54. Selvakannan, P.; Mandal, S.; Phadtare, S.; Pasricha, R.; Sastry, M. Capping of Gold Nanoparticles by the Amino Acid Lysine Renders Them Water-Dispersible. *Langmuir* **2003**, *19*, 3545–3549.
55. Lim, I. S.; Ip, W.; Crew, E.; Njoki, P. N.; Mott, D.; Zhong, C.-J.; Pan, Y.; Zhou, S. Q. Homocysteine-Mediated Reactivity and Assembly of Gold Nanoparticles. *Langmuir* **2007**, *23*, 826–833.
56. Ding, Y.; Xia, X. H.; Zhai, H. S. Reversible Assembly and Disassembly of Gold Nanoparticles Directed by a Zwitterionic Polymer. *Chem.—Eur. J.* **2007**, *13*, 4197–4202.
57. Si, S.; Mandal, T. K. pH-Controlled Reversible Assembly of Peptide-Functionalized Gold Nanoparticles. *Langmuir* **2007**, *23*, 190–195.
58. Nam, J.; Won, N.; Jin, H.; Chung, H.; Kim, S. pH-Induced Aggregation of Gold Nanoparticles for Photothermal Cancer Therapy. *J. Am. Chem. Soc.* **2009**, *131*, 13639–13645.
59. Kairdolf, B. A.; Nie, S. Multidentate-Protected Colloidal Gold Nanocrystals: pH Control of Cooperative Precipitation and Surface Layer Shedding. *J. Am. Chem. Soc.* **2011**, *133*, 7268–7271.
60. Zhou, K.; Liu, H.; Zhang, S.; Huang, X.; Wang, Y.; Huang, G.; Sumer, B. D.; Gao, J. Multicolored pH-Tunable and Activatable Fluorescence Nanoplatform Responsive to Physiologic pH Stimuli. *J. Am. Chem. Soc.* **2012**, *134*, 7803–7811.
61. Liu, X.; Zhu, H.; Jin, Q.; Zhou, W.; Colvin, V. L.; Ji, J. Small and Stable Phosphorylcholine Zwitterionic Quantum Dots for Weak Nonspecific Phagocytosis and Effective Tat Peptide Functionalization. *Adv. Healthcare Mater.* **2013**, *2*, 352–360.
62. Holmlin, R. E.; Chen, X. X.; Chapman, R. G.; Takayama, S.; Whitesides, G. M. Zwitterionic SAMs that Resist Nonspecific Adsorption of Protein from Aqueous Buffer. *Langmuir* **2001**, *17*, 2841–2850.
63. Chen, S. F.; Yu, F. C.; Yu, Q. M.; He, Y.; Jiang, S. Y. Strong Resistance of a Thin Crystalline Layer of Balanced Charged Groups to Protein Adsorption. *Langmuir* **2006**, *22*, 8186–8191.
64. Chen, S. F.; Jiang, S. Y. A New Avenue to Nonfouling Materials. *Adv. Mater.* **2008**, *20*, 335–338.
65. Liu, X.; Jin, Q.; Ji, Y.; Ji, J. Minimizing Nonspecific Phagocytic Uptake of Biocompatible Gold Nanoparticles with Mixed Charged Zwitterionic Surface Modification. *J. Mater. Chem.* **2012**, *22*, 1916–1927.
66. Yang, H.; Heng, X.; Hu, J. Salt-and pH-Resistant Gold Nanoparticles Decorated with Mixed-Charge Zwitterionic Ligands, and Their pH-Induced Concentration Behavior. *RSC Adv.* **2012**, *2*, 12648–12651.
67. Chen, S.; Zheng, J.; Li, L.; Jiang, S. Strong Resistance of Phosphorylcholine Self-Assembled Monolayers to Protein Adsorption: Insights into Nonfouling Properties of Zwitterionic Materials. *J. Am. Chem. Soc.* **2005**, *127*, 14473–14478.
68. Cao, Z.; Jiang, S. Ultralow-Fouling, Functionalizable, and Hydrolyzable Zwitterionic Materials and Their Derivatives for Biological Applications. *Adv. Mater.* **2010**, *22*, 920–932.
69. Mi, L.; Bernards, M. T.; Cheng, G.; Yu, Q.; Jiang, S. pH Responsive Properties of Non-Fouling Mixed-Charge Polymer Brushes Based on Quaternary Amine and Carboxylic Acid Monomers. *Biomaterials* **2010**, *31*, 2919–2925.
70. Nowinski, A. K.; Sun, F.; White, A. D.; Keefe, A. J.; Jiang, S. Sequence, Structure, and Function of Peptide Self-Assembled Monolayers. *J. Am. Chem. Soc.* **2012**, *134*, 6000–6005.
71. Yang, W.; Zhang, L.; Wang, S. L.; White, A. D.; Jiang, S. Y. Functionalizable and Ultra Stable Nanoparticles Coated with Zwitterionic Poly(carboxybetaine) in Undiluted Blood Serum. *Biomaterials* **2009**, *30*, 5617–5621.
72. Muro, E.; Pons, T.; Lequeux, N.; Fragola, A.; Sanson, N.; Lenkei, Z.; Dubertret, B. Small and Stable Sulfobetaine Zwitterionic Quantum Dots for Functional Live-Cell Imaging. *J. Am. Chem. Soc.* **2010**, *132*, 4556–4557.
73. Schlenoff, J. B.; Estephan, Z. G.; Jaber, J. A. Zwitterion-Stabilized Silica Nanoparticles: Toward Nonstick Nano. *Langmuir* **2010**, *26*, 16884–16889.
74. Park, J.; Nam, J.; Won, N.; Jin, H.; Jung, S.; Jung, S.; Cho, S. H.; Kim, S. Compact and Stable Quantum Dots with Positive, Negative, or Zwitterionic Surface: Specific Cell Interactions and Non-Specific Adsorptions by the Surface Charges. *Adv. Funct. Mater.* **2011**, *21*, 1558–1566.
75. Kataoka, K.; Lee, Y.; Fukushima, S.; Bae, Y.; Hiki, S.; Ishii, T. A Protein Nanocarrier from Charge-Conversion Polymer in Response to Endosomal pH. *J. Am. Chem. Soc.* **2007**, *129*, 5362–5363.

76. Zhou, K.; Wang, Y.; Huang, X.; Luby-Phelps, K.; Sumer, B. D.; Gao, J. Tunable, Ultrasensitive pH-Responsive Nanoparticles Targeting Specific Endocytic Organelles in Living Cells. *Angew. Chem., Int. Ed.* **2011**, *50*, 6109–6114.
77. Xie, J.; Xu, C.; Kohler, N.; Hou, Y.; Sun, S. Controlled PEGylation of Monodisperse Fe_3O_4 Nanoparticles for Reduced Non-Specific Uptake by Macrophage Cells. *Adv. Mater.* **2007**, *19*, 3163–3166.
78. Papasani, M. R.; Wang, G.; Hill, R. A. Gold Nanoparticles: The Importance of Physiological Principles to Devise Strategies for Targeted Drug Delivery. *Nanomed. Nanotechnol. Biol. Med.* **2012**, *8*, 804–814.
79. De Jong, W. H.; Hagens, W. I.; Krystek, P.; Burger, M. C.; Sips, A. J. A. M.; Geertsma, R. E. Particle Size-Dependent Organ Distribution of Gold Nanoparticles after Intravenous Administration. *Biomaterials* **2008**, *29*, 1912–1919.
80. Jain, T. K.; Foy, S. P.; Erokwu, B.; Dimitrijevic, S.; Flask, C. A.; Labhasetwar, V. Magnetic Resonance Imaging of Multifunctional Pluronic Stabilized Iron-Oxide Nanoparticles in Tumor-Bearing Mice. *Biomaterials* **2009**, *30*, 6748–6756.
81. Shin, D. M.; Huang, X. H.; Peng, X. H.; Wang, Y. Q.; Wang, Y. X.; El-Sayed, M. A.; Nie, S. M. A Reexamination of Active and Passive Tumor Targeting by Using Rod-Shaped Gold Nanocrystals and Covalently Conjugated Peptide Ligands. *ACS Nano* **2010**, *4*, 5887–5896.
82. Chan, W. C. W.; Chithrani, B. D. Elucidating the Mechanism of Cellular Uptake and Removal of Protein-Coated Gold Nanoparticles of Different Sizes and Shapes. *Nano Lett* **2007**, *7*, 1542–1550.
83. Elghanian, R.; Storhoff, J. J.; Mucic, R. C.; Letsinger, R. L.; Mirkin, C. A. Selective Colorimetric Detection of Polynucleotides Based on the Distance-Dependent Optical Properties of Gold Nanoparticles. *Science* **1997**, *277*, 1078–1081.
84. Harris, T. J.; von Maltzahn, G.; Derfus, A. M.; Ruoslahti, E.; Bhatia, S. N. Proteolytic Actuation of Nanoparticle Self-Assembly. *Angew. Chem., Int. Ed.* **2006**, *45*, 3161–3165.